Influence of the magnetic sublattices in the double perovskite $LaCaNiReO_6$

Konstantinos Papadopoulos,[1] Ola Kenji Forslund,[1,2] Elisabetta Nocerino,[2] Fredrik O. L. Johansson,[3,4,5] Gediminas Simutis,[1,6] Nami Matsubara,[2] Gerald Morris,[7] Bassam Hitti,[7] Donald Arseneau,[7] Peter Svedlindh,[8] Marisa Medarde,[9] Daniel Andreica,[10] Jean-Christophe Orain,[11] Vladimir Pomjakushin,[12] Lars Börjesson,[1] Jun Sugiyama,[13] Martin Månsson,[2] and Yasmine Sassa[1,*]

[1]*Department of Physics, Chalmers University of Technology, SE-412 96 Göteborg, Sweden*
[2]*Department of Applied Physics, KTH Royal Institute of Technology, SE-106 91 Stockholm, Sweden*
[3]*Division of Molecular and Condensed Matter Physics, Uppsala University, SE-752 37 Uppsala, Sweden*
[4]*Division of Applied Physical Chemistry, KTH Royal Institute of Technology, SE-100 44 Stockholm, Sweden*
[5]*Sorbonne Universite, UMR CNRS 7588, Institut des Nanosciences de Paris, F-75005 Paris, France*
[6]*Laboratory for Neutron and Muon Instrumentation, Paul Scherrer Institut, CH-5232 Villigen PSI, Switzerland*
[7]*TRIUMF, 4004 Wesbrook Mall, Vancouver, BC, V6T 2A3, Canada*
[8]*Uppsala University, Department of Materials Science and Engineering, Uppsala University, 751 03 Uppsala, Sweden*
[9]*Laboratory for Multiscale Materials Experiments, Paul Scherrer Institut, CH-5232 Villigen PSI, Switzerland*
[10]*Faculty of Physics, Babes-Bolyai University, 400084 Cluj-Napoca, Romania*
[11]*Laboratory for Muon Spin Spectroscopy, Paul Scherrer Institute, CH-5232 Villigen PSI, Switzerland*
[12]*Laboratory for Neutron Scattering and Imaging, Paul Scherrer Institute, CH-5232 Villigen PSI, Switzerland*
[13]*Neutron Science and Technology Center, Comprehensive Research Organization for Science and Society (CROSS), Tokai, Ibaraki 319-1106, Japan*

(Received 11 April 2022; revised 25 June 2022; accepted 16 September 2022; published 8 December 2022)

The magnetism of double perovskites is a complex phenomenon, determined from intra- or interatomic magnetic moment interactions, and strongly influenced by geometry. We take advantage of the complementary length and timescales of the muon spin rotation, relaxation, and resonance (μ^+SR) microscopic technique and bulk ac/dc magnetic susceptibility measurements to study the magnetic phases of the $LaCaNiReO_6$ double perovskite. As a result, we are able to discern and report ferrimagnetic ordering below $T_C = 102$ K and the formation of different magnetic domains above T_C. Between $T_C < T < 270$ K, the following two magnetic environments appear, a dense spin region and a static-dilute spin region. The paramagnetic state is obtained only above $T > 270$ K. An evolution of the interaction between Ni and Re magnetic sublattices, in this geometrically frustrated fcc perovskite structure, is revealed as a function of temperature through the critical behavior and thermal evolution of microscopic and macroscopic physical quantities.

DOI: 10.1103/PhysRevB.106.214410

I. INTRODUCTION

In the research on multifunctional materials, oxides with a double perovskite structure are continuously attracting our interest due to their structural malleability and a multitude of complex physical properties that arise through their magnetically frustrated geometry [1,2]. Properties such as a magnetoelectric effect, magnetocaloric effect, magnetoresistance or superconductivity may appear in the various phases of perovskite oxides [3–5]. If we are to tune and make use of these properties for real life applications in magnetoelectronics and spintronics, the challenge lies in revealing the static and dynamic processes driven from spin reorientation.

The general composition of this class of materials, illustrated in Fig. 1(a), is $AA'BB'O_6$ where A, A' are alkaline earth or lanthanide cations, and B, B' are $3d$, $4d$ or $5d$ transition metals (TMs) in various oxidation states. The AA' and B, B' 1:1 ratios provide an ordering of $BO_6, B'O_6$ edge-sharing octahedra which form two crystallographically distinct sublattices [6,7]. The structure is flexible to expand, contract or distort from cation displacements, the Jahn-Teller effect or tilting of the octahedra. These distortions are responsible for changes in character of superexchange interactions (ferromagnetic-antiferromagnetic) [8,9] or the appearance of Dzyaloshinski-Moriya (DM) interactions [10], which significantly alter the physical properties of the perovskite [11]. The magnetic phases of these compounds are controlled both by

*yasmine.sassa@chalmers.se

Published by the American Physical Society under the terms of the Creative Commons Attribution 4.0 International license. Further distribution of this work must maintain attribution to the author(s) and the published article's title, journal citation, and DOI. Funded by Bibsam.

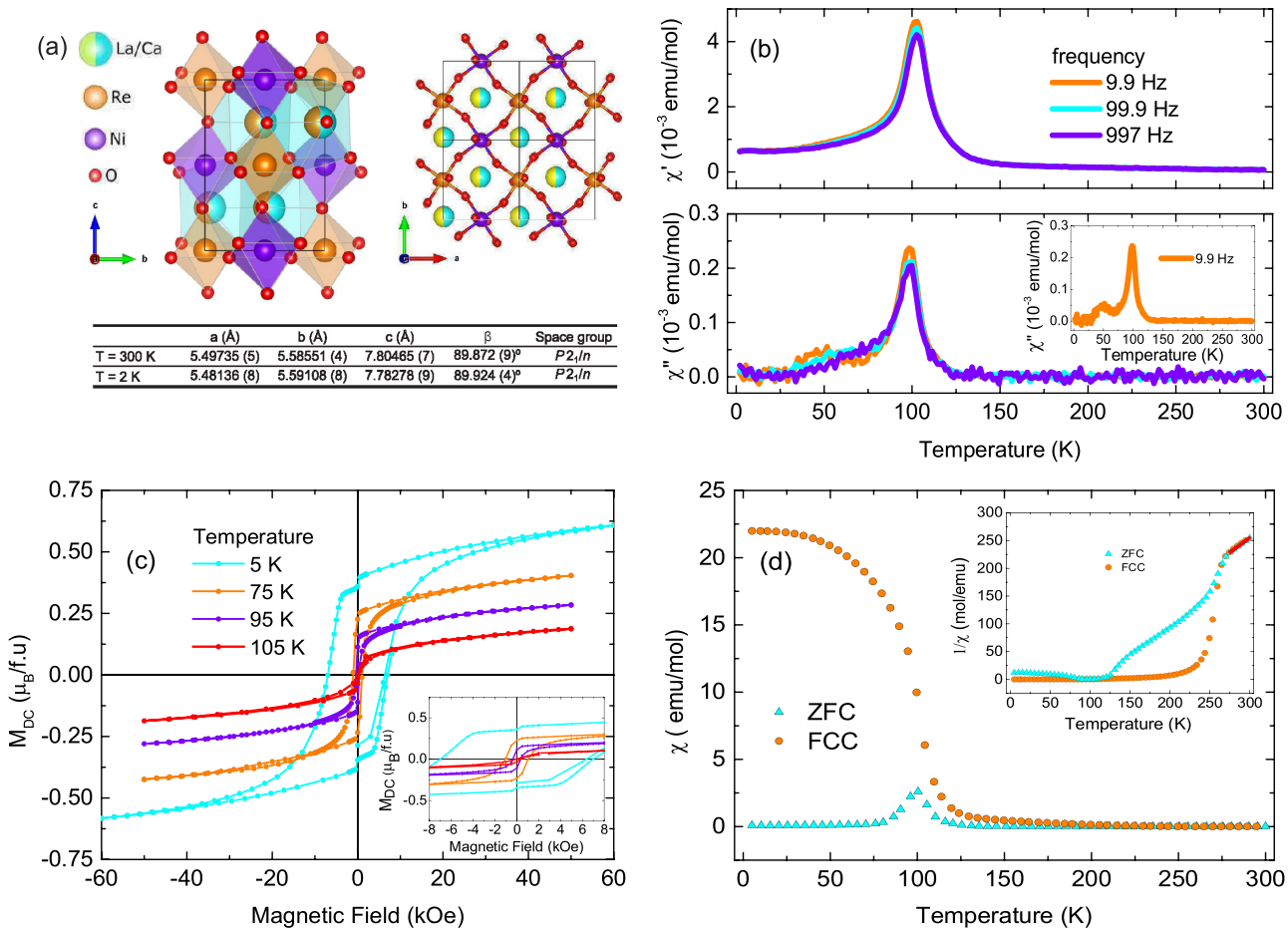

	a (Å)	b (Å)	c (Å)	β	Space group
T = 300 K	5.49735 (5)	5.58551 (4)	7.80465 (7)	89.872 (9)°	$P2_1/n$
T = 2 K	5.48136 (8)	5.59108 (8)	7.78278 (9)	89.924 (4)°	$P2_1/n$

FIG. 1. (a) The crystal structure of $LaCaNiReO_6$, a geometrically frustrated face-centered cubic, monoclinic crystal lattice that accommodates alternating Ni-O and Re-O octahedra. (b) The real and imaginary component of ac susceptibility vs temperature for different frequencies. The evolution of χ'' susceptibility at 9.9 Hz is also shown independently for clarity. (c) Magnetic hysteresis loops for 5, 75, 95, and 105 K. The inset focuses around the remanence and coercive field regions. (d) Temperature dependence of dc magnetic susceptibility in ZFC and FCC sequences. The inset presents the inverse magnetic susceptibility.

the magnetic and nonmagnetic cations present. More specifically, the sublattice symmetries, the cation's nominal spin and its spin-orbit coupling (SOC) as well as exchange interactions, are degrees of freedom that determine the magnetic ground state [12].

A particularly interesting double perovskite compound is the $LaCaNiReO_6$. This material is the sister compound of $LaSrNiReO_6$ [13], and contrary to other double perovskite compounds [14], the *AA'* positions in the crystal structure are occupied randomly by either La^{3+} or Ca^{2+}. The *BB'* positions are also occupied by two different cations, Ni^{2+} and Re^{5+} that, at variance with the *A* cations, form an ordered, rock salt-type network or corner-sharing octahedra [Fig. 1(a)]. In transition metal (TM) perovskite oxides, where nearest neighbor TM cations are connected by oxygen sites, superexchange is usually the dominant magnetic interaction. In general, these interactions control the sign and magnitude of the couplings, which depend on the TM orbital filling and the *B-O-B'* bond angle. According to the Goodenough-Kanamori (GKA) rules, the interaction is the strongest at 180° and is antiferromagnetic if the virtual electron (e^-) transfer is between overlapping orbitals that are each half filled, but ferromagnetic if the virtual e^- transfer is from a half filled to an empty orbital or from filled to half filled orbital. At 90°, the interaction is the weakest and it is favored to be ferromagnetic [15]. For $LaCaNiReO_6$, the *B-O-B'* bonds are bent to an angle of 152° at 1 K [8]. Between the half filled e_g orbitals of Ni^{2+} and partially filled t_{2g} orbitals of Re^{5+}, the interaction should favor an antiferromagnetic coupling between nearest neighbors (NN) Ni-Re. In addition there exists a competition between these NN interaction and the longer range, next nearest neighbors (NNN) Ni-Ni and Re-Re. For the 180° NNN bonds, according to GKA, a ferromagnetic coupling is possible [16]. Neutron powder diffraction (NPD) refinement reflects a ground state that is determined by two interacting magnetic sublattices where the Ni spins orient antiparallel to the Re spins, while the moments of each individual sublattice order along the same direction [8].

In this study, we employed both muon spin rotation/relaxation/resonance (μ^+SR) and magnetometry techniques to scrutinize the phases of magnetic ordering in this compound. Muons as local probes can extract space

and time dependent information of the material's intrinsic magnetic environment in zero applied fields. A muon spin precession frequency is a direct indication of an ordered state, while the spin relaxation provides information of the ordering range and fluctuations [17]. Since the time window of muons is typically 10^{-12}–10^{-6} s, these results are correlated to ac and dc magnetization measurements that provide a bulk view of the sample in a 10^{-6}–1 s time window, thus taking into account fast and slow magnetic fluctuations that may occur.

Our results show a ferrimagnetic transition to a long-range and commensurate ordered state, below $T_C = 102$ K. The ferrimagnetic ordering has been proposed in previous studies [8], but our μ^+SR results suggest that its origin is based on cooperative effects of each sublattices. At higher temperatures the sublattices are independent of one another, but as the sample is cooled down the interaction between them results into the ferrimagnetic order. Moreover, a small anomaly is observed around 70 K and we suggest different scenarios for its origin. Above T_C, the μ^+SR and magnetization results support the existence of two co-existing magnetic phases from 102 up to 270 K, while from 270 K up to room temperature the paramagnetic phase takes over.

II. EXPERIMENTAL DETAILS

A polycrystalline sample of $LaCaNiReO_6$ was prepared in stoichiometric ratio by solid state synthesis. La_2O_3, $SrCO_3$, $CaCO_3$, NiO, Re_2O_7, and Re metal were used as the starting materials, forming the final compound through mixing, grinding, pelleting and sintering cycles. X-ray and neutron diffraction patterns were recorded at 300, 125, and 1 K to verify the composition. The $P2_1/n$ structural model fits the NPD data at all temperatures, manifesting the absence of a structural phase transition going across the magnetic ordering, based on the resolution of the given NPD data. More information about the synthesis and structure characterization can be found in Ref. [8].

AC-DC magnetization measurements over a 5−300 K temperature range were carried out in a zero-field cooled (ZFC), field-cooled while cooling (FCC) and field-cooled while warming (FCW) process. Magnetic field scans were also performed in a −60 to + 60 kOe magnetic field range, at various temperatures. The instruments used were a Quantum Design Physical Property Measurement System (PPMS) with a vibrating sample magnetometry setup (VSM) as well as a Magnetic Property Measurement Systems (MPMS) Superconducting Quantum Intereference Device (SQUID).

The μ^+SR experiments were performed at the surface muon beamline **M20** in the TRIUMF facilities. A 100% polarized, continuous, positive muon beam was targeted onto an aluminium coated mylar envelope of approximately 1 cm^2 surface, filled with ∼1 g of the powdered sample. The sample was inserted in a ^{4}He cryostat and reached a 2 K base temperature. The software package *musrfit* was used to analyze the data [18]. Measurements were performed in the zero field (ZF), longitudinal field (LF), and transverse field (TF) geometry, with respect to the initial muon spin polarization. Muons are implanted one at a time into the sample, and come to rest at an interstitial site. There, their spins interact with the local magnetic field, undergoing a Larmor precession and finally emit a positron, with a high probability in the direction of the spin orientation before decay [17]. Our data sets consist of ∼10 million positron counts for the TF and LF measurements, and ∼35 million counts for the ZF measurements.

III. RESULTS

A. Magnetic susceptibility

Temperature dependent dc magnetic susceptibility was measured at 5–300 K with an applied field of 100 Oe, as shown in Fig. 1(d). The FCC and FCW (not displayed) curves were identical meaning that there was no quenching of magnetic moments during the cooling. The bifurcation between the FCC and ZFC curves reveals a change in the magnetic response of the system around 270 K. The FCC susceptibility at low temperatures reveals a ferromagnetic component and from its first derivative we determined a critical Curie temperature $T_C^{\chi} = 100.3(3)$ K. To extend the results of the previous study [8] below the Curie temperature, we show explicitly that the ZFC susceptibility reaches the value of 0.08 emu/mol at 5K for an 100 Oe applied field. The ZFC susceptibility increases with increasing temperature and obtains a maximum close to the derived Curie temperature. The ZFC and FCC inverse susceptibility is presented in the inset of Fig. 1(d). The region above transition could not be fitted with a hyberbola according to Neel's molecular field model [19]. Consequently, we fitted the linear region at 270 K $< T <$ 300 K to the Curie-Weiss law $\frac{1}{\chi} = \frac{T-\theta}{C}$ [20]. The fit resulted to a Curie constant of $C = 0.94(2)$ K and Curie temperature $\theta = 60(4)$ K. The ZFC-FCC curve types below transition and the calculated Curie temperature value are characteristic features of a ferrimagnetic ordering. The effective magnetic moment was then calculated from $\mu_{\text{eff}} = 2.83(\frac{C_m}{Z})^{\frac{1}{2}}\mu_B$, where C_m the molar Curie constant, Z the formula unit per unit cell and μ_B the Bohr magneton [21]. The effective moment is $\mu_{\text{eff}} = 0.63\ \mu_B$. If we consider unquenched or partially quenched orbital moments for the Re and Ni ions in the octahedral complexes, the total μ_{eff} is given by $\mu_{\text{eff}}^2 = xg^2J(J+1)\mu_B^2$, where x the fraction of magnetic ions per formula unit, g their gyromagnetic factor and J the total angular momentum. Assuming that the Ni^{2+} and Re^{5+} magnetic systems have the same ordering temperature through superexchange coupling [22,23], we calculate $\mu_{\text{eff}} = \sqrt{\mu_{\text{eff.Ni}}^2 - \mu_{\text{eff.Re}}^2} = 1.03\ \mu_B$, where $\mu_{\text{eff.Ni}} = 1.81\ \mu_B$ and $\mu_{\text{eff.Re}} = 1.49\ \mu_B$. This theoretical value is an overestimation to the experimentally extracted values from our magnetization measurements but in good agreement with the values obtained from the neutron diffraction refined peaks from Ref. [8]. The precision of the spin only determination of magnetic moment is of course limited since spin-orbit coupling in Re ions, Jahn-Teller distortions of Re-O octahedra and the possible canted magnetic structure will affect the spontaneous magnetization of the compound.

Isothermal field dependent dc magnetization measurements were performed at 5, 75, 95, 105, and 300 K for magnetic fields from −60 to +60 kOe. The evolution of the magnetization is presented in Fig. 1(c) (the paramagnetic, linear behavior at 300 K is not shown). Magnetization saturation is never reached for ferrimagnets, however at the maximum field of 60 kOe, we consider an effective magnetic moment of

$\mu_{\text{eff5K}} = 0.60\ \mu_B$ at 5 K, following the previous experimental values. A long-range order is evident and a very large coercive field (≈7 kOe) is measured. High coercivity and remanence have been also observed in other Re-based double perovskites [24–26] and was attributed to an intrinsic anisotropy of these compounds. Taking into account a strong SOC of Re ions, first-principles calculations [27] predict a large unquenched orbital moment, which is thought to be the origin of the magnetic anisotropy [28]. In the 5-K hysteresis loop, shoulders appear at zero field. In the recorded loops at 75 K and above, these shoulders disappear and the remanence and coercivity diminish with increasing temperature. Similar kinks have been observed in systems exhibiting spin reorientation [29,30] or superparamagentic spins [31]. In our case however, signs of spin reorientation is not aparent in the magnetization or in the μ^+SR data. Instead, a recent theoretical study showed that magnetic anisotropy could in certain conditions also result in an anomaly in the hysteresis loop [32]. Since the presence of this anomaly is temperature dependent, it seems the interaction between Ni and Re is different at 5 K compared to $T > 75$ K. This is further discussed below.

Ac magnetic susceptibility measurements were also performed at three ac field frequencies on a bias field of 200 Oe, to probe the magnetic relaxation in the two sublattice spin system as shown in Fig. 1(b). The ordering temperature does not depend on the frequency and a spin glass behavior is excluded. We observe that a second peak in the χ'' susceptibility curve rises at 50 K as the frequency is tuned from 1000 to 10 Hz.

B. Muon spin rotation

The μ^+SR study consists of weak TF, ZF and LF measurements. We can extract the local field distribution from the time spectra of the emitted positron asymmetries between the surrounding detectors [33,34]. From the TF spectra we extract the initial and baseline asymmetry which are used as constants when treating the ZF time spectra. The fitted asymmetry from the TF spectra maps the magnetic transition through the dephasing of the external signal. The ZF and LF measurements follow in order to gain detailed information about the conditions of magnetic ordering, as well as the intrinsic magnetic fields, arising from nuclear and electronic moments.

1. Weak transverse field (TF)

Muon depolarization spectra were recorded for TF = 50 Oe in the temperature range 2 K $\leqslant T \leqslant$ 300 K. We present the evolution of the TF spectra at selected temperatures, above and below the magnetic phase transition in Fig. 2(a). The time spectra exhibits oscillatory and non oscillatory signals. Therefore the TF time spectra were fitted using an exponentially relaxing oscillatory component and an exponentially relaxing nonoscillatory component according to

$$A_0\, P_{\text{TF}}(t) = A_{\text{TF}} \cos(2\pi f t + \phi) e^{-\lambda_{\text{TF}} t} + A_S e^{-\lambda_S}, \quad (1)$$

where A_0 is the initial asymmetry and P_{TF} is the muon spin polarization function. A_{TF}, f, ϕ and λ_{TF} are the asymmetry, frequency, relative phase and depolarization rate of the implanted muon's spins under applied TF, while A_S and λ_S account for muon spin depolarization due to the sample's internal magnetic field. We observe a damping of the oscillation with decreasing temperature, towards a magnetically ordered

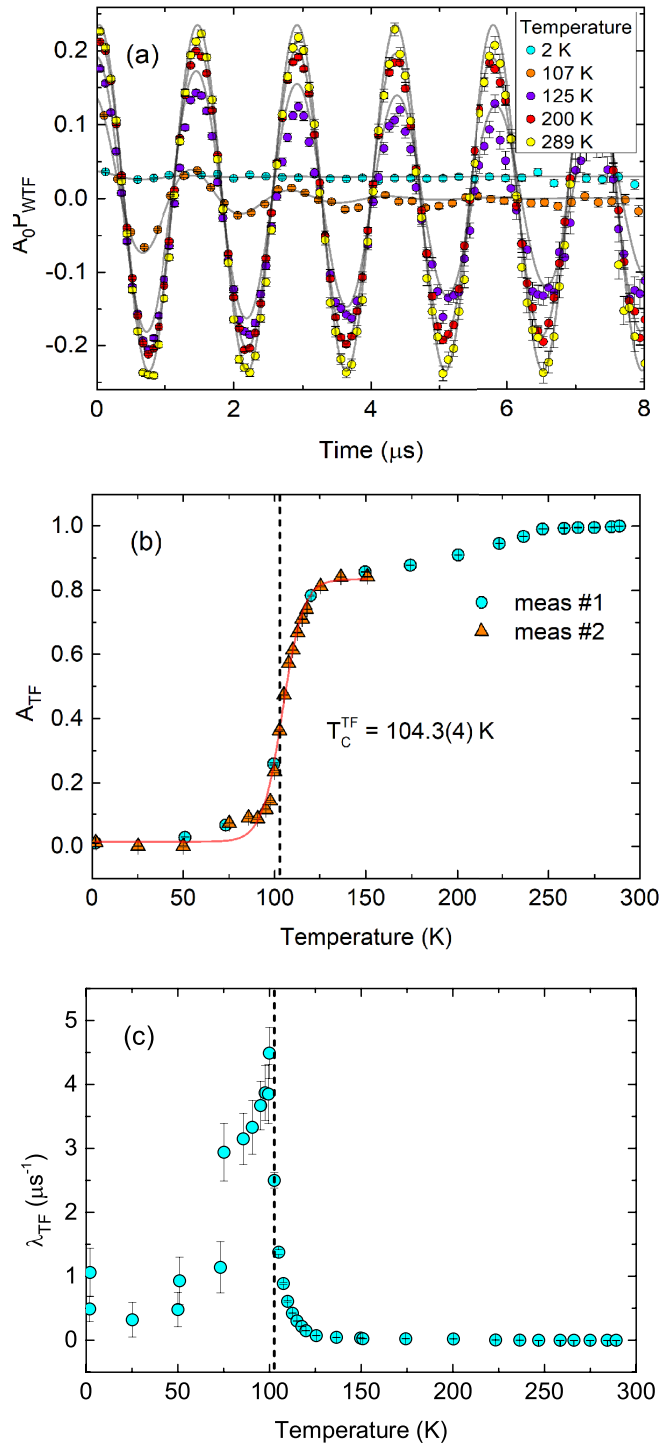

FIG. 2. (a) Weak transverse field (TF = 50 Oe) time spectra recorded at $T = 2$, 107, 125, 200, and 289 K. The solid lines are fits obtained from Eq. (1). (b) The TF asymmetry as a function of temperature. The main transition temperature, $T_C^{\text{TF}} = 104.3(4)$ K, is defined at the point in the middle of the transition and is obtained via a fit using the sigmoid function (solid line). (c) The relaxation rate of the oscillatory component as a function of temperature.

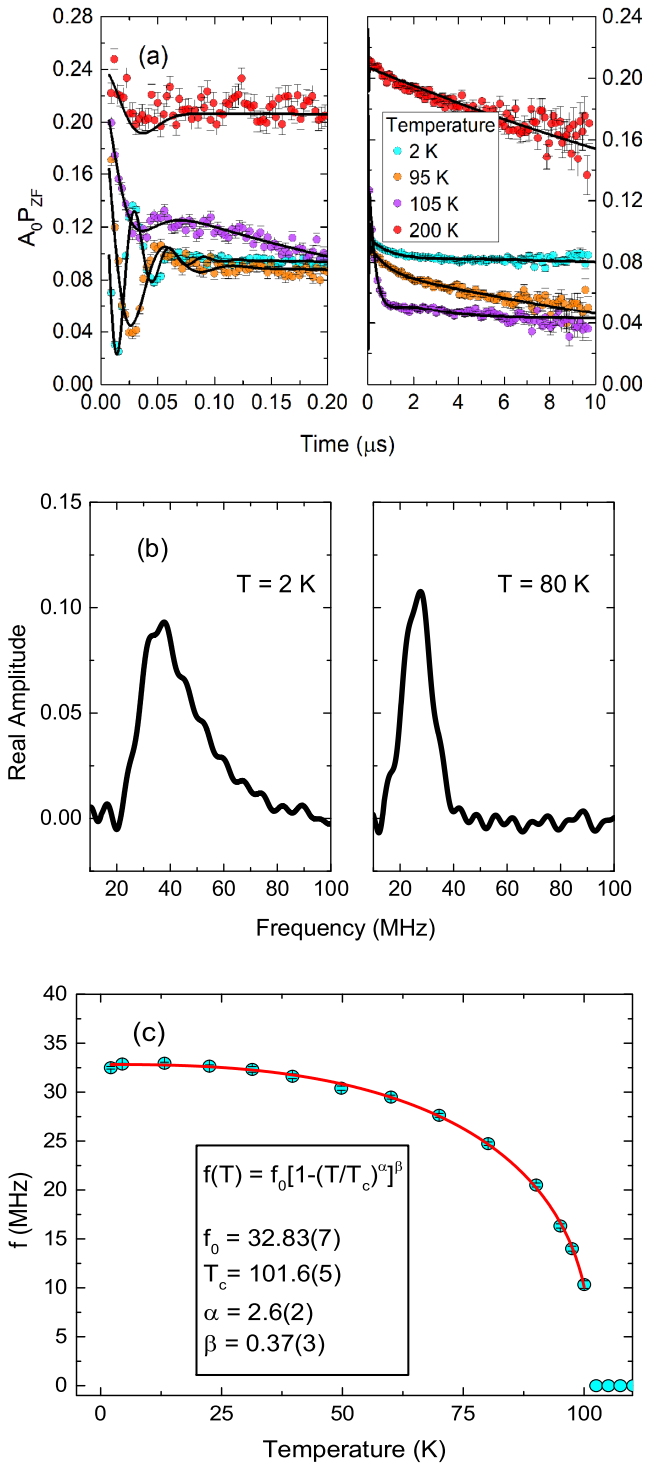

FIG. 3. (a) Zero field time spectra collected at 2, 95, 105, and 200 K where the solid lines corresponds to fits with Eq. (2) and/or Eq. (4). The left and right window present the short and long time domain of the ZF time spectrum, respectively. (b) The real part of the Fourier transform of the μ^+SR time spectrum collected at 2 and 80 K. (c) Temperature dependence of the muon spin presession frequency, obtained using Eq. (2) for $n = 1$. The solid line represents the best fit using Eq. (3), as also shown in the inset.

state. The oscillation frequency is proportional to the applied magnetic field while the asymmetry $A_{\rm TF}$ corresponds to the externally magnetized fraction of the sample. The transverse field asymmetry is displayed as a function of temperature in figure Fig. 2(b) and is fitted with a Boltzmann sigmoid function, yielding a transition temperature of $T_{\rm C}^{\rm TF} = 104.3(4)$ K.

The obtained TF fit parameters are shown in Fig. 2. The internal field contributions, $A_{\rm S}$ and $\lambda_{\rm S}$, are omitted as more detailed information about the internal field is presented in the ZF section below. Above $T_{\rm C}$, the sample enters a dilute phase (discussed below) and a paramagnetic phase is achieved above 270 K where the asymmetry is fully recovered, a behavior that corroborates the dc susceptibility results. The depolarization rate $\lambda_{\rm TF}$ is presented in Fig. 2(c). At high temperatures above $T_{\rm C}$, the fluctuations of the local magnetic moments increase and as a result, the rate approaches zero due to a motional narrowing. When temperature is decreased, $\lambda_{\rm TF}$ displays a peak around the magnetic phase transition, pointing towards a slowing down of the magnetic fluctuations.

2. *Zero field (ZF)*

ZF measurements were carried out in the temperature range 2 K $\leqslant T \leqslant$ 200 K. We present a selection of muon spin depolarization spectra at temperatures above and below the magnetic transition in Fig. 3(a). In the short timescale, the onset of a precession and a fast relaxation of the muon spin ensemble appears below 102 K. This damped oscillation is the effect of a static internal field distribution, perpendicular to the muon spin. At base temperature $T = 2$ K a cosinusoidal oscillation appears up to 0.10 μs, which denotes a commensurate magnetic ordering. In the long timescale, a slower relaxation describes the spin dynamics which correspond to the longitudinal field components to the muon spin.

a. Below the transition temperature. The time spectrum is fitted with two oscillating components, one slowly relaxing component [35] and one temperature independent background component up to 105 K:

$$A_0\, P_{\rm ZF}(t) = \sum_n^2 A_{\rm n}^{\rm FI} \cos(2\pi f_{\rm n} t + \phi_{\rm n}) e^{-\lambda_{\rm n}^{\rm T} t} + A_{\rm tail} e^{-\lambda_{\rm tail} t} + A_{\rm imp} e^{-\lambda_{\rm imp} t}, \quad (2)$$

where $A_n^{\rm FI}$ is the asymmetry, $\lambda_{\rm n}^{\rm T}$ is the depolarization rate, f the frequency, which is a measure of the sublattice magnetization, and $\phi_{\rm n}$ is the phase of the muon spin depolarization, originating from perpendicular internal magnetic field components with respect to the initial muon spin polarization. $A_{\rm tail}$ and $\lambda_{\rm tail}$ are the asymmetry and depolarization rate originating from internal field components that are parallel with respect to the initial muon spin polarization. In a powder sample, 2/3 of the asymmetry is expected to be oscillating ($A_1^{\rm FI} + A_2^{\rm FI}$) while the rest, 1/3, is expected to depolarize in a slow manner, *i.e.* the tail component ($A_{\rm tail}$).

From density functional theory (DFT) calculations on the sister compound $LaSrNiReO_6$, up to two possible muon sites were predicted [13]. The ZF time spectra collected for the title compound at 2 K clearly exhibit one single frequency, which is heavily damped [Figs. 3(a) and 3(b)]. A fit with a single oscillation is able to reproduce the detailed oscillation [Fig. 3(c)], however adding a second frequency improves the fit and the following frequencies are obtained $f_1 = 35.6(6)$ MHz and $f_2 = 29.2(4)$ MHz. In fact, local field

calculations, assuming only dipolar contribution [36,37], based on the solved magnetic structure [8] using ordered moments $\mu_{Re} = 0.5\ \mu_B$ and $\mu_{Ni} = 1.5\ \mu_B$ result in $f_1^{calc} = 38.4$ MHz $\simeq f_1$ and $f_2^{calc} = 28.9$ MHz $\simeq f_2$. These results suggest the presence of two separate frequencies in our time spectrum. The asymmetric shape of the Fourier transform at 2 K [Fig. 3(b)] supports the scenario as well. Therefore, on the assumption that there are two muon sites, we fit the time spectra with two frequencies, according to Eq. (2).

Since the internal field distribution is wide, some constraints are set in the fitting procedure in order to obtain accurate fit parameters. The phase between the frequencies were set as a common parameter, $\phi_n = \phi$. Moreover, the impurity asymmetry was fixed to the value obtained at 2 K; $A_{imp} = 0.0142(5)$, which corresponds to approximately 5.9% of the sample. This value is also consistent with the TF measurements, in which a small fraction was oscillating even at base temperature. The ratio between A_1^{FI} and A_2^{FI} was also fixed to the value of 0.41, obtained at base temperature. These assumptions are based on the fact that a commensurate magnetic order is expected, as well as no structural transitions were reported in high resolution neutron diffraction measurements [8].

Figures 3(c) and 4(b) show the obtained frequencies as a function of temperature by using only one or two ZF muon spin precession frequencies in the fitting procedure described above. When considering two frequencies, these become indistinguishable around 70 K and merge into one component. Most likely, both frequencies are still present but f_1 and f_2 are so close in frequencies that they cannot be separated. This assessment is also supported by the FFT from the 80 K measurement [Fig. 3(b)]. At 80 K, the field distribution width is narrower and also symmetric compared with the one collected at 2 K, even though one would expect wider distributions closer to the transition ($T_C = 102$ K). This behavior suggests the presence of two components at 2 K that merge around 70 K and the origin to this merging is discussed below.

Focusing first on Fig. 3(c), the frequency is proportional to the sample magnetization and the experimental data can be fitted by a power-law function [11,17,38] that considers both spontaneous magnetization and spin-wave excitations at low temperatures, but also the magnetic anisotropy that becomes significant near the Curie temperature:

$$f(T) = f_0\left[1 - \left(\frac{T}{T_C}\right)^{\alpha}\right]^{\beta}, \tag{3}$$

where f_0 is proportional to the spontaneous magnetization at base temperature. The critical exponent α corresponds to the low temperature properties, and β determines the asymptotic behavior near the transition temperature. The fit results to a critical temperature $T_C = 101.6(5)$ K. This is the actual critical temperature of the sample since the ZF measurement probes the intrinsic magnetic ordering without excitations. The critical exponent $\beta = 0.37(3)$ matches to the 3D Heisenberg model, while the low temperature exponent $\alpha = 2.6(2)$ follows the $T^{5/2}$ power law according to the Dyson formalism [39]. This behavior describes a system of two spin waves interacting in a ferromagnet. In case of a ferrimagnet, the magnon excitation includes transverse fluctuations of both sublattice spins and the dispersion curve consists of two branches [40,41].

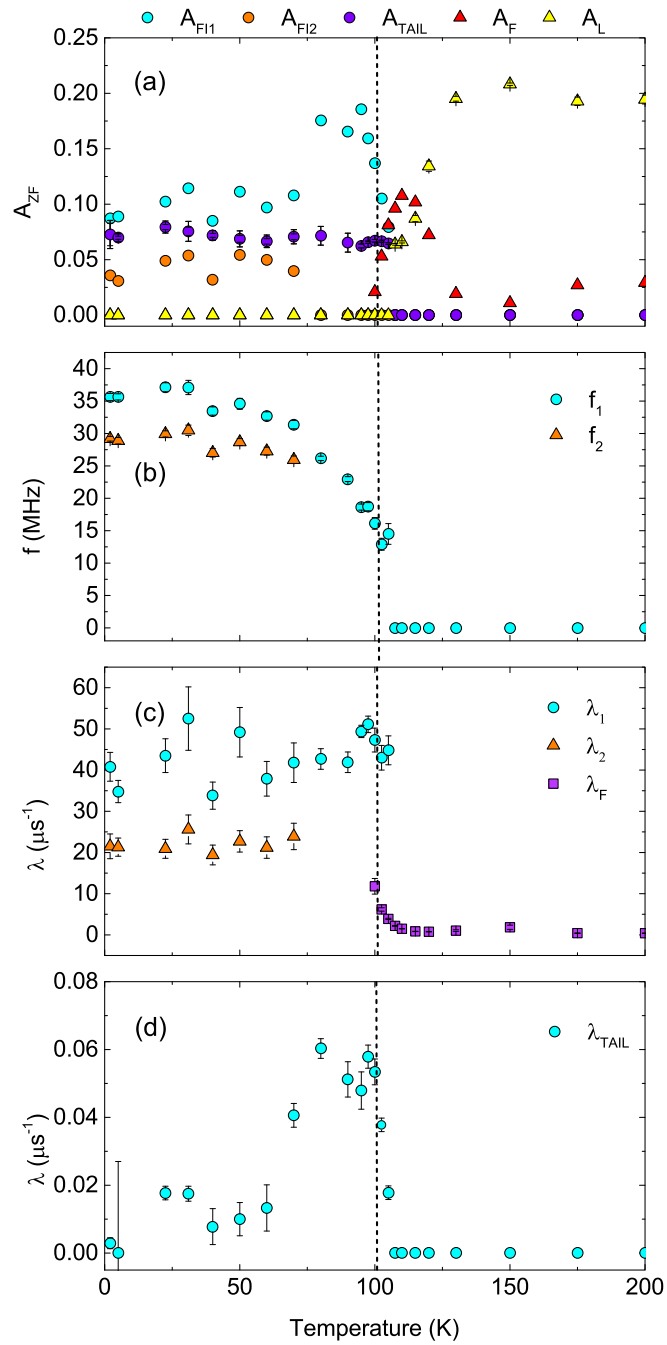

FIG. 4. Zero field (ZF) temperature dependent fit parameters obtained using Eq. (2) and/or Eq. (4): (a) asymmetries (A_{FI1}, A_{FI2}, A_{tail}, A_F, and A_L), (b) precession frequencies (f_1 and f_2), (c) fast relaxation rates (λ_1, λ_2, and λ_F), and (d) slow relaxation rate (λ_{tail}).

Now moving on Fig. 4(a), below T_C, A_n^{FI} and A_{tail} are temperature independent and maintain the 2/3 and 1/3 ratios. The rise in A_1^{FI} around 70 K corresponds to the fact that the two frequency components merges into one and the asymmetry weight is taken from A_2^{FI} to A_1^{FI}. In the temperature region from 95 K and up to T_C, the asymmetry of A_1^{FI} (oscillation) decreases and is taken over by A_F (exponential). This means

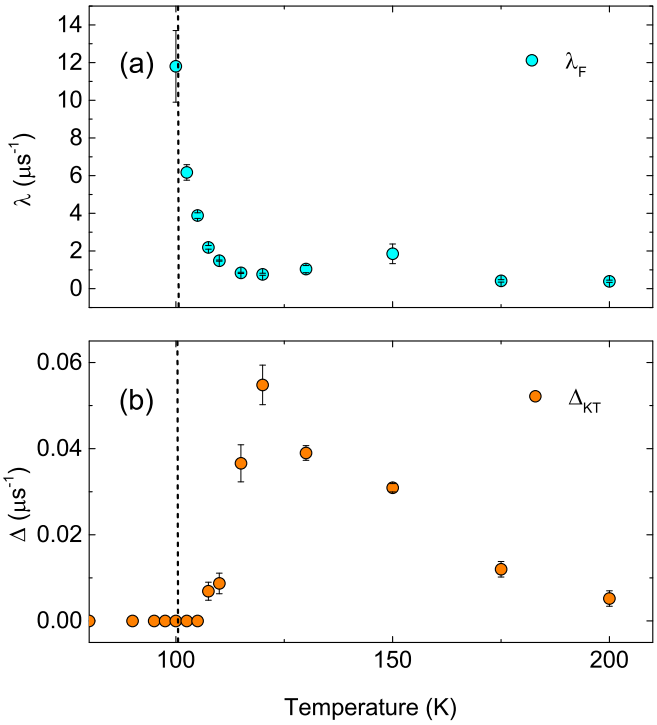

FIG. 5. Temperature dependence of the obtained ZF fit parameters using Eq. (4): (a) the relaxation rate of the fast component and (b) the field distribution width of the Lorentzian KT.

that there exist a small temperature region in which oscillations coexists with a fast relaxing component. This behavior is quite unusual [37] and is further discussed below. The depolarization rates λ_n^T and λ_{tail} increase as the temperature approaches the transition, revealing an increase in internal magnetic field dynamics. λ_n^T ($n = 1, 2$) have high values down to base temperature since they depend on the static field distribution width [Fig. 4(c)]. The longitudinal component on the other hand slowly approaches zero as the thermal fluctuations are suppressed at lower temperatures [Fig. 4(d)]. The evolution of λ_{tail}, a measure of spin-lattice relaxation rate, can be described as a function of temperature $aT^2 \ln(T)$ below T_C. This dependence has been identified to be a signature of muon depolarization from a two magnon excitation [42,43], consistent with the power law magnetization model.

b. Above the transition temperature. From 95 to 200 K, the ZF-μ^+SR spectra consist of rapidly and slowly relaxing parts [Fig. 3(a)] in the short- and long-time domains of the zero field time spectra. Therefore they were parameterized using a combination of an exponential and a static Lorentzian Kubo-Toyabe function (L_{KT}) [44]:

$$A_0 P_{ZF}(t) = A_F e^{-\lambda_F t} + A_L L_{KT}^{stat}(\Delta, t). \quad (4)$$

This kind of relaxation function was also used to describe $LaSrNiReO_6$ [13] above the transition temperature. The fast relaxing part [Fig. 5(a)] is related to magnetic domains or possibly a short-range ordering present in the sample, revealed also by the $M(H)$ measurement. The slow relaxing part [Fig. 5(b)] describes a partly paramagnetic state enriched with dilute magnetic moments. The asymmetries A_F and A_L are a measure of the volume fractions of the magnetic and paramagnetic regions, respectively. With increasing temperature the magnetic regions are diminished (A_F) and the partial paramagnetic state (A_L) is eventually prevalent [Fig. 4(a)]. It is noted that A_F is the reason why A_{TF} does not recover the whole asymmetry above the transition. Overall, the value of A_F suggests that 25% of the volume is characterized by electronic moments in a dynamic state. This value is consistent with the wTF-μ^+SR result, in which about 20% of the sample is in a magnetic state at temperatures between 150 and 270 K [see Fig. 2(b)]. It is also noted that λ_F exhibits a local maximum at 150 K [Fig. 5(a)], a phenomenon similar to the one observed in the sister compound $LaSrNiReO_6$ [13] and the origin is currently unknown.

This complex magnetic arrangement was further examined by measuring the longitudinal field dependence of the μ^+SR spectra at 175 K. The ZF- and LF-μ^+SR spectra under fields of 20, 34, and 60 Oe are presented in Fig. 6(b). The LF-μ^+SR spectra are found to be successfully fitted with Eq. (4). A clear decoupling behavior is observed for the longer time domain, an indication of a static but random field distribution. It is noted that a single Gaussian KT cannot describe the measured spectra under LF.

IV. DISCUSSION

Both conventional bulk magnetic susceptibility and microscopic μ^+SR experiments were used to complete the picture of the magnetically diverse double perovskite $LaCaNiReO_6$ down to a commensurate, long-range ferrimagnetic order established below $T_C = 102$ K. The underlying inter- and intrasublattice exchange interactions between first, second or higher order neighbors define the magnetic ground state. Alterations to the electron configuration, as a result of spin orbit coupling, the Jahn-Teller effect as well as the composition of the crystal lattice, will result to a frustrated structure. In our case, exchange for a relatively smaller alkaline earth metal results to a different ground state to the one realized in its sister compound $LaSrNiReO_6$, for which an incommensurate magnetic ground state was suggested [13]. These two compounds are a characteristic example proving that frustration together with superexchange interaction play a definitive role in the magnetic ordering of perovskite oxides.

As GKA rules predict, for a 152° Ni-O-Re angle, there exists an antiferromagnetic (AF) exchange interaction between Ni^{2+} and Re^{5+} ions, a signature of geometrical frustration. The long-range Ni-Ni and Re-Re interactions in the two sublattices are also significant, as they were described in a similar case for $LaSrNiRuO_6$ [16]. The NNN couplings are expected to be of ferromagnetic nature, leading to ferromagnetically ordered sublattices that are antiferromagnetically coupled. In parallel, the strong spin-orbit coupling of Re atoms, in comparison to Ni ones, ehances the total magnetic moment of the former but also facilitates a DM exchange interaction and antisymmetric superexchange coupling [45], leaving open the possibility to observe frozen spin components perpendicular to the ferrimagnetic order [46,47].

In our experiments, we followed the evolution of magnetic phases with temperature. Based on the temperature dependent ZF-μ^+SR results (Fig. 4), we conclude that,the sample enters

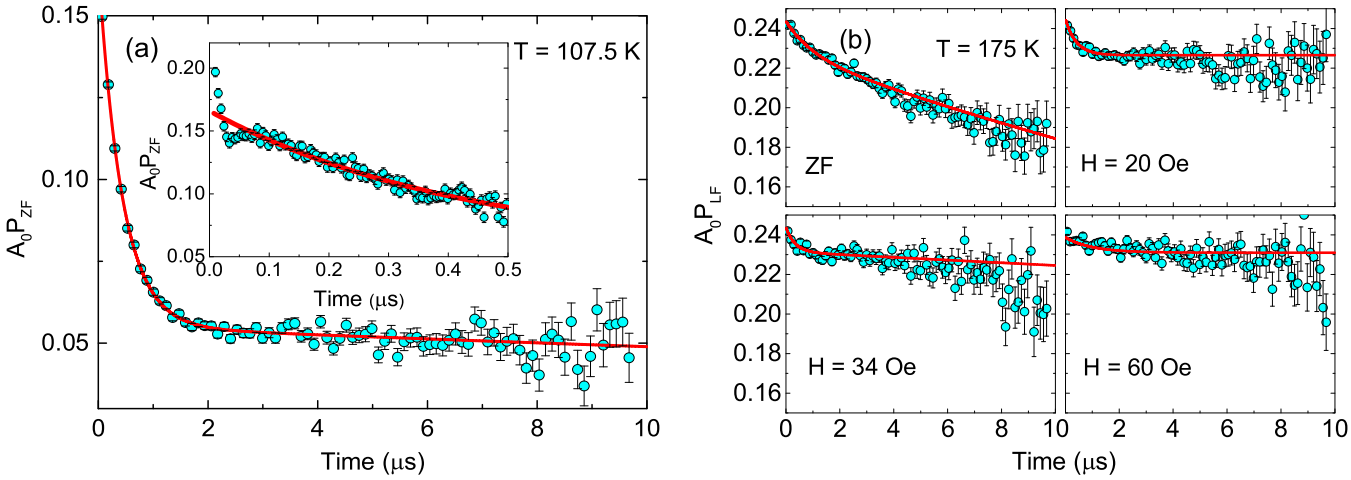

FIG. 6. (a) Zero field time spectra at $T = 107.5$ K fitted with Eq. (4). The inset shows the depolarization function at early times. (b) The zero and longitudinal field depolarization spectra for LF = 20, 34, and 60 Oe, at $T = 175$ K, also fitted with Eq. (4).

a long-range magnetic order below T_C. The depolarization lineshape consists of a highly damped oscillation and a slowly relaxing part with the corresponding 2/3 and 1/3 ratios, as expected for a powder sample. The TF measurements (Fig. 2) revealed that the full asymmetry is not recovered until above $T = 270$ K where the sample enters the paramagnetic state.

In the $T_C < T < 270$ K region, a mixed magnetic phase appears. This evolution is corroborated by the inverse dc susceptibility [Fig. 1(d)] behavior until we reach the temperature region described by the Curie-Weiss law. Both results hint towards a non-single-phase sample. In fact, μ^+SR time spectra above T_C was described by Eq. (4), that is a fast relaxing exponential and a Lorenzian KT. Since L-KT is the dilute limit of the KT, commonly observed in paramagnets with dilute magnetic moments [48], A_F can be attributed to muons situated close to these dilute fluctuating magnetic moments. In the sister compound, $LaSrNiReO_6$ [13], it was proposed that the dilute Re moments are fluctuating/interacting at higher temperature. As the temperature is lowered, Ni interactions become significant, effectively destroying the dilute limit to eventually realize a long-range magnetic order. Presumably, a similar description also holds for $LaCaNiReO_6$.

Another scenario to describe the two magnetic phases above T_C can be attributed to coexistence of two crystalline phases. A study of the magnetically similar compound, Ca_2FeReO_6, hinted at a mesoscopic phase separation in two monoclinic phases that coexist in a wide temperature range, with different magnetic properties [24]. If a similar situation is applicable to $LaCaNiReO_6$, the A_F and A_L contributions are understood to originate from these two crystalline phases. The appearance of two phases can be justified as a result of magnetostriction due to changes in the distance and angle of the *B-O-B'* bonds. Although, we wish to note that crystalline phase separation was not observed in both high resolution XRD and NPD measurements.

We now focus on the magnetic ordering below T_C. Below T_C the Ni and Re sublattices order [8,49,50] and the critical exponents extracted from this transition follow the 3D Heisenberg model. For the ferrimagnet, this model consists of two coupled ferromagnetic sublattices with unequal and antiparallel magnetic moments. The molecular field consists of three coefficients, two ferromagnetic for each sublattice and one antiferromagnetic for their interaction. Around 70 K the two muon spin precession frequency components are merged into one component [Fig. 4(b)]. This temperature region is comparable to the one where a peak was observed in ac susceptibility and these two phenomena are most likely related to each other. First off, any changes in the number of frequency components in μ^+SR is typically related to changes in the magnetic structure [51]. Although, a simple canting of the magnetic structure does not change the number of frequency components in this case. Instead, the data suggest that the two frequencies become so close that they cannot be distinguished. In fact, asserting the same ordered moment size on Re and Ni, i.e., $\mu_{Re} = \mu_{Ni}$, results into one frequency in local field calculations. Therefore we may initially suggest that the reason of the decrease in the number of components is because Ni and Re moments becomes comparable. Considering the SOC of Re, it is reasonable to assume that the Ni moment is suppressed faster with temperature and eventually reaches the value of Re. At this point, another interaction between Ni and Re moments may become significant and change their fluctuation characteristics, which in turn result in a peak in ac susceptibility.

Another way of interpreting the data is by assuming that either the Re or the Ni moments are partly disordered/fluctuating above 70 K. In this case, one of the moments (Ni or Re) first orders at T_C and the second one orders below 70 K. The two sublattices are thus independent above 70 K and this picture is partly supported by the fact that the spin-lattice relaxation rate (λ_{tail}) exhibits a sudden drop around 70 K. This kind of lattice specific dynamics were observed in another double perovskite compound, Sr_2CoOsO_6 [52]. In this case, the Co moments order first and the Os orders at lower temperatures. In this kind of ordering, the ac-susceptibility exhibits a clear peak [52], similar to what is shown in Fig. 1(b). Although, in this scenario, one would perhaps expect one of the oscillations to turn into a fast relaxing exponential, as also seen for Sr_2CoOsO_6 [52]. With this said, we would like to point out that there is a small temperature

region in which an oscillation and a fast relaxing components coexist: from 97.5 K up to T_C [Fig. 4(a)]. Therefore the partial ordering of one of the sublattice scenario may be applicable not at 70 K but above 97.5 K. This kind of coexistence between oscillation and exponential is quite unusual [37].

V. CONCLUSIONS

We have utilized magnetometry and muon spin spectroscopy to elucidate the magnetic properties of the double perovskite compound $LaCaNiReO_6$. Due to Ni and Re sublattice interactions, magnetic phases appear as early as $T <$ 270 K. With decreasing temperature these phases evolve and finally a transition into a commensurate ferrimagnetic order occurs below $T_C = 102$ K. As a result of two magnetic sublattices, we find that the interaction between them changes as a function of temperature. While Re fluctuations dominate above T_C, the Ni moments start to contribute at lower temperatures and in collaboration with Re moments result into a ferrimagnetic order. We also observe smaller anomaly around 70 K and discussed various scenarios for its origin. It is a suggestive observation, that although both $LaCa_xSr_{1-x}NiReO_6$, $x = 1, 0$ share a common dense and dilute magnetic phase above their magnetic order transition and up to 270 K, the substitution of a larger with a smaller diameter alkaline-earth drastically facilitates or hinders the formation of magnetic order at low temperatures.

ACKNOWLEDGMENTS

This research was supported by the European Commission through a Marie Skłodowska-Curie Action and the Swedish Research Council - VR (Dnr. 2014-6426 and 2016-06955) as well as the Carl Tryggers Foundation for Scientific Research (CTS-18:272). J.S. acknowledge support from Japan Society for the Promotion Science (JSPS) KAKENHI Grant Nos. JP18H01863 and JP20K21149. Y.S. and O.K.F are funded by the Swedish Research Council (VR) through a Starting Grant (Dnr. 2017-05078) and E.N. by the Swedish Foundation for Strategic Research (SSF) within the Swedish national graduate school in neutron scattering (SwedNess). Y.S. and K.P. acknowledge funding from the Area of Advance- Material Sciences from Chalmers University of Technology. D.A. acknowledges partial financial support from the Romanian UEFISCDI Project No. PN-III-P4-ID-PCCF-2016-0112. G.S. acknowledges funding from the Chalmers X-Ray and Neutron Initiatives (CHANS) grant and European Union's Horizon 2020 research and innovation program under the Marie Skłodowska-Curie Grant Agreement No. 884104 (PSI-FELLOW-III-3i). F.O.L.J acknowledges support from the Swedish Research Council - VR (Dnr. 2020-06409). The MPMS used to perform the measurements at the LMX laboratory of the Paul Scherrer Institute was supported by the Swiss National Science Foundation through Grant No. 206021-139082. All images involving crystal structure were made with the VESTA software [53].

[1] P. M. Woodward, Acta Crystallogr. Sect. B **53**, 32 (1997).
[2] V. Pardo and W. E. Pickett, Phys. Rev. B **80**, 054415 (2009).
[3] D. T. Marx, P. G. Radaelli, J. D. Jorgensen, R. L. Hitterman, D. G. Hinks, S. Pei, and B. Dabrowski, Phys. Rev. B **46**, 1144 (1992).
[4] K.-I. Kobayashi, T. Kimura, H. Sawada, K. Terakura, and Y. Tokura, Nature **395**, 677 (1998).
[5] B. Stojanovic, C. Jovalekic, V. Vukotic, A. Simoes, and J. A. Varela, Ferroelectrics **319**, 65 (2005).
[6] M. Singh, K. Truong, S. Jandl, and P. Fournier, J. Appl. Phys. **107**, 09D917 (2010).
[7] Y. M. Klein, M. Kozłowski, A. Linden, P. Lacorre, M. Medarde, and D. J. Gawryluk, Cryst. Growth Des. **21**, 4230 (2021).
[8] S. Jana, P. Aich, P. A. Kumar, O. K. Forslund, E. Nocerino, V. Pomjakushin, M. Månsson, Y. Sassa, P. Svedlindh, O. Karis *et al.*, Sci. Rep. **9**, 18296 (2019).
[9] A. A. Aczel, D. E. Bugaris, L. Li, J.-Q. Yan, C. de la Cruz, H.-C. zur Loye, and S. E. Nagler, Phys. Rev. B **87**, 014435 (2013).
[10] W. K. Zhu, C. K. Lu, W. Tong, J. M. Wang, H. D. Zhou, and S. X. Zhang, Phys. Rev. B **91**, 144408 (2015).
[11] C. Thompson, J. Carlo, R. Flacau, T. Aharen, I. Leahy, J. Pollichemi, T. Munsie, T. Medina, G. Luke, J. Munevar *et al.*, J. Phys.: Condens. Matter **26**, 306003 (2014).
[12] X. Ding, B. Gao, E. Krenkel, C. Dawson, J. C. Eckert, S.-W. Cheong, and V. Zapf, Phys. Rev. B **99**, 014438 (2019).
[13] O. K. Forslund, K. Papadopoulos, E. Nocerino, G. Morris, B. Hitti, D. Arseneau, V. Pomjakushin, N. Matsubara, J.-C. Orain, P. Svedlindh *et al.*, Phys. Rev. B **102**, 144409 (2020).
[14] T. Shang, E. Canévet, M. Morin, D. Sheptyakov, M. T. Fernández-Díaz, E. Pomjakushina, and M. Medarde, Sci. Adv. **4**, eaau6386(2018).
[15] J. Kanamori, J. Phys. Chem. Solids **10**, 87 (1959).
[16] X. Ou, F. Fan, X. Chen, T. Li, L. Jiang, A. Stroppa, X. Ouyang, and H. Wu, Europhys. Lett. **123**, 57003 (2018).
[17] A. Yaouanc and P. D. De Reotier, *Muon Spin Rotation, Relaxation, and Resonance: Applications to Condensed Matter* (Oxford University Press, 2010).
[18] A. Suter and B. Wojek, Phys. Procedia **30**, 69 (2012).
[19] J. S. Smart, Am. J. Phys. **23**, 356 (1955).
[20] M. A. de Vries, A. C. Mclaughlin, and J. W. G. Bos, Phys. Rev. Lett. **104**, 177202 (2010).
[21] J. Yang and Y. Lee, J. Korean Phys. Soc. **51**, 1560 (2007).
[22] S. de Brion, F. Ciorcas, G. Chouteau, P. Lejay, P. Radaelli, and C. Chaillout, Phys. Rev. B **59**, 1304 (1999).
[23] R. Gupta, I. N. Bhatti, and A. Pramanik, J. Phys.: Condens. Matter **32**, 035803 (2020).
[24] J. M. De Teresa, D. Serrate, J. Blasco, M. R. Ibarra, and L. Morellon, Phys. Rev. B **69**, 144401 (2004).
[25] H. Kato, T. Okuda, Y. Okimoto, Y. Tomioka, Y. Takenoya, A. Ohkubo, M. Kawasaki, and Y. Tokura, Appl. Phys. Lett. **81**, 328 (2002).
[26] T. Alamelu, U. V. Varadaraju, M. Venkatesan, A. P. Douvalis, and J. M. D. Coey, J. Appl. Phys. **91**, 8909 (2002).
[27] H.-T. Jeng and G. Y. Guo, Phys. Rev. B **67**, 094438 (2003).
[28] F. Bloch and G. Gentile, Z. Phys. **70**, 395 (1931).
[29] M. Ahmed, N. Imam, M. Abdelmaksoud, and Y. Saeid, J. Rare Earth **33**, 965 (2015).

[30] S. Heisz, G. Hilscher, H. Kirchmayr, H. Harada, and M. Tokunaga, IEEE Trans. Magn. **23**, 3110 (1987).
[31] W. Pei, D. Zhao, C. Wu, X. Wang, K. Wang, J. Wang, and Q. Wang, RSC Adv. **9**, 36034 (2019).
[32] T. Magno de Lima Alves, B. F. Amorim, M. A. Morales Torres, C. G. Bezerra, S. Nóbrega de Medeiros, P. L. Gastelois, L. E. Fernandez Outon, and W. Augusto de Almeida Macedo, RSC Adv. **7**, 22187 (2017).
[33] P. D. De Reotier and A. Yaouanc, J. Phys.: Condens. Matter **9**, 9113 (1997).
[34] R. L. Garwin, L. M. Lederman, and M. Weinrich, Phys. Rev. **105**, 1415 (1957).
[35] S. J. Blundell, P. A. Pattenden, F. L. Pratt, R. M. Valladares, T. Sugano, and W. Hayes, Europhys. Lett. **31**, 573 (1995).
[36] O. K. Forslund, H. Ohta, K. Kamazawa, S. L. Stubbs, O. Ofer, M. Månsson, C. Michioka, K. Yoshimura, B. Hitti, D. Arseneau *et al.*, Phys. Rev. B **102**, 184412 (2020).
[37] O. K. Forslund, D. Andreica, H. Ohta, M. Imai, C. Michioka, K. Yoshimura, M. Månsson, and J. Sugiyama, Phys. Scr. **96**, 125864 (2021).
[38] R. Pełka, P. Konieczny, M. Fitta, M. Czapla, P. Zieliński, M. Bałanda, T. Wasiutyński, Y. Miyazaki, A. Inaba, D. Pinkowicz *et al.*, Acta Phys. Pol. A **124**, 977 (2013).
[39] D. C. Mattis, *The Theory of Magnetism I* (Springer Berlin Heidelberg, 2012).
[40] N. Karchev, J. Phys.: Condens. Matter **20**, 325219 (2008).
[41] H. Kaplan, Phys. Rev. **86**, 121 (1952).
[42] P. Gubbens, P. D. De Réotier, A. Yaouanc, A. Menovsky, and C. Snel, Hyperfine Interact. **85**, 245 (1994).
[43] D. Beeman and P. Pincus, Phys. Rev. **166**, 359 (1968).
[44] R. Feyerherm, A. Amato, C. Geibel, F. N. Gygax, P. Hellmann, R. H. Heffner, D. E. MacLaughlin, R. Muller-Reisener, G. J. Nieuwenhuys, A. Schenk, and F. Steglich, Phys. Rev. B **56**, 699 (1997).
[45] T. Thio, T. R. Thurston, N. W. Preyer, P. J. Picone, M. A. Kastner, H. P. Jenssen, D. R. Gabbe, C. Y. Chen, R. J. Birgeneau, and A. Aharony, Phys. Rev. B **38**, 905 (1988).
[46] D. Ryan, J. Van Lierop, and J. Cadogan, J. Phys.: Condens. Matter **16**, S4619 (2004).
[47] D. H. Ryan, J. M. Cadogan, and J. van Lierop, Phys. Rev. B **61**, 6816 (2000).
[48] R. E. Walstedt and L. R. Walker, Phys. Rev. B **9**, 4857 (1974).
[49] C. R. Wiebe, J. E. Greedan, G. M. Luke, and J. S. Gardner, Phys. Rev. B **65**, 144413 (2002).
[50] J. Wang, W. Song, and Z. Wu, Phys. Status Solidi B **247**, 194 (2010).
[51] O. K. Forslund, D. Andreica, Y. Sassa, H. Nozaki, I. Umegaki, E. Nocerino, V. Jonsson, O. Tjernberg, Z. Guguchia, Z. Shermadini *et al.*, Sci. Rep. **9**, 1141 (2019).
[52] B. Yan, A. K. Paul, S. Kanungo, M. Reehuis, A. Hoser, D. M. Többens, W. Schnelle, R. C. Williams, T. Lancaster, F. Xiao *et al.*, Phys. Rev. Lett. **112**, 147202 (2014).
[53] K. Momma and F. Izumi, J. Appl. Crystallogr. **44**, 1272 (2011).